

Dynamical Coulomb blockade of thermal transport

Guillem Rosselló,¹ Rosa López,¹ and Rafael Sánchez²

¹*Institut de Física Interdisciplinària i de Sistemes Complexos IFISC (CSIC-UIB), E-07122 Palma de Mallorca, Spain*

²*Instituto Gregorio Millán, Universidad Carlos III de Madrid, 28911 Leganés, Madrid, Spain*

(Dated: September 20, 2018)

The role of energy exchange between a quantum system and its environment is investigated from the perspective of the Onsager conductance matrix. We consider the thermoelectric linear transport of an interacting quantum dot coupled to two terminals under the influence of an electrical potential and a thermal bias. We implement in our model the effect of coupling to electromagnetic environmental modes created by nearby electrons within the $P(E)$ -theory of dynamical Coulomb blockade. Our findings relate the lack of some symmetries among the Onsager matrix coefficients with an enhancement of the efficiency at maximum power and the occurrence of the heat rectification phenomenon.

I. INTRODUCTION

The properties of electronic heat transport in nanostructures have recently attracted the attention of the scientific community for different reasons^{1–3}. On one hand, the onset of quantum effects in the mesoscopic regime opens the way to the investigation of the impact of quantum mechanics on thermodynamics.⁴ In particular, heat engines based on purely quantum mechanical effects have been recently proposed.^{5–10} Complementary to this, there has been a spectacular progress in the field of quantum thermoelectrics, both from the theoretical and experimental sides. Exciting proposals like nanoprobe thermometers^{1,11}, energy harvesting devices^{12–16}, refrigerators^{17–21}, heat diodes²², rectifiers^{23–26}, transistors^{27,28}, multi-terminal heat engines^{29–32} among others have come up in the last years.

In this respect, quantum dots^{33–42} have a prominent role for being good energy filters that improve the thermoelectric efficiency^{43,44}. The presence of strong interactions introduces the Coulomb blockade regime where transport can be controlled at the level of single-electron tunneling events^{45,46}. Different functionalities such as heat engines¹⁴, pumps^{47–49} and diodes²² can be defined that use these properties.

Currents are small in nanostructures, and are hence sensible to fluctuations. The question arises of how the system behaviour is influenced by a noisy environment. On one hand, it leads to dephasing and decoherence which are detrimental to quantum coherent processes. This is however not necessarily negative^{50,51}. On the other hand, they may lead to inelastic transitions which can contribute to the engine performance by injecting or releasing energy in the conductor^{52–54}. Indeed, non-local thermoelectric engines exist that use an environment as a heat source in an otherwise equilibrated conductor. The nature of the environment can either be fermionic^{55,56} or bosonic^{29,57}. It can also consist of transport fluctuations in a Coulomb coupled conductor^{58–61} or be due to quantum fluctuations in an electromagnetic environment^{62,63}. This last effect has been observed in the form of the dynamical Coulomb blockade of charge currents^{64–68}.

The linear response of a two terminal nanodevice is defined on the grounds of the Onsager-Casimir relations^{69–71}. The Onsager coefficients $\mathcal{O}_{ij} = \partial \mathcal{I}_i / \partial \mathcal{A}_j$ relate the charge and heat fluxes $\mathcal{I}_i \equiv \{I_i^e, I_i^h\}$ in terminal i to the thermodynamic affinities \mathcal{A}_j . These can be due to electric or thermal gradients. Shortly, the coefficients \mathcal{O}_{ij} can be collected into the so-called Onsager conductance matrix which is a symmetric and positively semi-defined matrix.⁷² Derived from the principle of microreversibility, Onsager reciprocity relations identify non diagonal coefficients \mathcal{O}_{ij} , e.g. Seebeck and Peltier responses. Notoriously, such relations are also satisfied for quantum systems independently on the presence of interactions. For quantum systems in which phase coherence is preserved, additional relations for the Onsager coefficients are obtained from the unitarity of the electron dynamics^{73,74} giving rise to highly symmetric Onsager matrices. However, environment-system energy exchange events prevent the dynamics to be unitary. In particular some relations among the thermoelectric coefficients are no longer satisfied.^{55,75} The microscopic origin of such asymmetries has so far not been discussed.

In this work we explore this issue by using a micro-

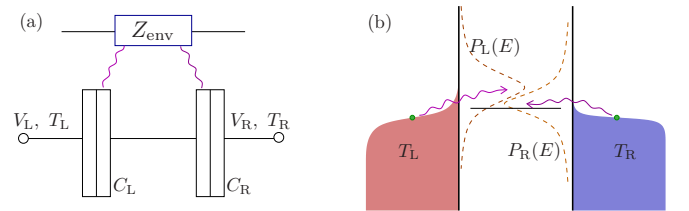


FIG. 1. (a) Schematic of a two terminal single-level quantum dot device in the presence of an electromagnetic environment described by an external impedance $Z_{\text{env}}(\omega)$. Each terminal is electrically and thermally biased with V_L , $T_L = T_0 + \Delta T_L$ (left contact) and V_R , $T_R = T_0 + \Delta T_R$ (right contact). The capacitance associated to each junction, C_i , determines the dynamical coupling to the environment. (b) Inelastic tunneling into the quantum dot is then described by a distribution $P_j(E)$ which is different for each barrier.

scopic model for the coupling of a mesoscopic system to a dynamical environment⁷⁶. We consider the simplest situation of a single-level quantum dot tunnel-coupled to two terminals, L and R. Particle tunneling between two quantum states is accomplished by energy exchange with an electromagnetic environment that describes the vacuum fluctuations. The environment is modeled by an external impedance, as sketched in Fig. 1. This results in photon-assisted tunneling events which on top of becoming inelastic, introduce left-right asymmetric rates. As we show below, the occurrence of Onsager matrix asymmetries is due to combination of these two effects. It leads to responses that do not only depend on the global temperature gradient $\Delta T = T_L - T_R$ but rather on how it is distributed with respect to some reference temperature T_0 in the two leads, $\Delta T_l = T_l - T_0$. It affects the thermoelectric response and most particularly, it introduces an apparent thermal rectification in the linear regime.

The remaining of the manuscript is organized as follows. In Sec. II our model is described. Results for the single and double occupation regimes are presented in Secs. III and IV, respectively, with conclusions discussed in Sec. V.

II. THEORETICAL MODEL

We consider a two terminal interacting conductor as illustrated in Fig. 1. We use a spinful single level quantum dot described by four states $|0\rangle$, $|u\rangle$, $|d\rangle$ and $|2\rangle$. They correspond to an empty dot ($|0\rangle$), a singly occupied dot with either spin up ($|u\rangle$) or down ($|d\rangle$) polarization, and the doubly occupied dot state ($|2\rangle$). Our transport description is restricted to the sequential tunneling regime for which $\Gamma \ll k_B T_0$ (T_0 is the temperature). In this regime, transport events are predominantly of the first order in the tunneling coupling Γ . To properly account for Coulomb interactions we employ the electrostatic model schematically illustrated in Fig. 1. In such model, the electrostatic charging energy is described with two capacitances C_L and C_R . The dynamics of the system is modeled by the time evolution of the occupation probabilities $p \equiv \{p_0, p_u, p_d, p_2\}$ described by the general master equation

$$\frac{dp_i}{dt} = \sum_k (\Gamma_{i \leftarrow k} p_k - \Gamma_{k \leftarrow i} p_i). \quad (1)$$

Applied to our formalism this equation would read e.g. for p_0 :

$$\frac{dp_0}{dt} = \sum_j \left[-\Gamma_{j,0}^+ p_0 + \Gamma_{j,0}^- (p_u + p_d) \right], \quad (2)$$

whose transition rates are of the form $\Gamma_{j,s}^\pm$ for electrons tunneling *in* (-) or *out* (+) of the dot through contact j are given below. We do not consider a magnetic field, so they do not depend on spin. They depend on the electrochemical potential μ_s when the dot is empty $s = 0$ or

singly occupied $s = 1$. A simple electrostatic electrostatic model⁷⁷ yields

$$\mu_s = \epsilon_d + \frac{e^2(1+2s)}{2C} + e(\kappa_L V_L + \kappa_R V_R), \quad (3)$$

where ϵ_d is the bare energy level of the quantum dot, $C = C_L + C_R$ is its total capacitance, and $\kappa_j = 1 - C_j/C$, with $j = L, R$, see Fig. 1.

A. Tunneling rates

Tunneling events are frequently affected by fluctuations of the electromagnetic environment⁶⁸. To fully account for such quantum fluctuations we adopt the $P(E)$ theory^{68,76} of dynamical Coulomb blockade, recently revisited to consider heat fluxes⁶². The spirit of the $P(E)$ theory relies on the fact that individual tunneling events involve energy exchange processes. The Dirac-delta accounting for energy conservation in the (Fermi golden rule) tunneling rates is relaxed into a broadened distribution $P(E)$. More specifically for a double junction it reads

$$P_j(E) = \frac{1}{2\pi\hbar} \int dt \exp \left(\kappa_j^2 J(t) + \frac{i}{\hbar} Et \right). \quad (4)$$

where the function

$$J(t) = \frac{2\hbar}{e^2} \int_0^\infty \frac{d\omega}{\omega} \text{Re}[\tilde{Z}(\omega)] c(\omega, T_0), \quad (5)$$

contains all the information of the environment fluctuations, with⁷⁶:

$$c(\omega, T_0) = \coth \left(\frac{\hbar\omega}{2k_B T_0} \right) [\cos(\omega t - 1) - i \sin \omega t]. \quad (6)$$

If we consider a pure resistive or ohmic environment, i.e. we have

$$Z_{env}(\omega) = R \gg R_q = \hbar/2e^2. \quad (7)$$

This situation corresponds to the case where the electron tunnel may easily excite many electromagnetic modes. Thus, the total impedance seen by the external circuit is

$$\tilde{Z}(\omega) = [i\omega C_{\text{eff}} + Z_{env}(\omega)]^{-1}, \quad (8)$$

with the effective capacitance of the quantum dot $C_{\text{eff}}^{-1} = C_L^{-1} + C_R^{-1}$. Under these considerations the high impedance limit leads to a Gaussian distribution for $P_j(E)$:

$$P_j(E) = \frac{1}{\sqrt{4\pi\kappa_j^2 E_C k_B T_0}} e^{-\frac{(E - \kappa_j^2 E_C)^2}{4\kappa_j^2 E_C k_B T_0}}, \quad (9)$$

Here $E_C = q^2 \kappa_L \kappa_R / 2C$. Remarkably, asymmetries in the system capacitances translate in the $P_j(E)$ functions

having different mean, $\kappa_j^2 E_C$, and variance, $2\kappa_j^2 E_C k_B T_0$. They modify the transition rates expressions according to

$$\Gamma_{j,s}^\pm = \Gamma_j \int dE f^\pm(E - eV_j, T_j) P_j(E - \mu_s). \quad (10)$$

where $f^+(E, T) = 1/[1 + e^{E/(k_B T)}]$ is the Fermi function, and $f^- = 1 - f^+$. The tunneling rates can be left-right asymmetric for having barriers with different transparencies, $\Gamma_L \neq \Gamma_R$. We emphasize that, very differently, having $P_L(E) \neq P_R(E)$ introduces an implicit energy dependence. As we discuss below, the impact in the system response shows up in the thermal transport coefficients.

Finally, the charge and heat currents through contact j are calculated through

$$I_j^e = e \left[\sum_{\sigma=u,d} (\Gamma_{j,0}^+ - \Gamma_{j,1}^-) p_\sigma - \Gamma_{j,0}^- p_0 + \Gamma_{j,1}^+ p_2 \right] \quad (11)$$

$$I_{j\sigma}^h = \sum_{\sigma=u,d} (\gamma_{j,0}^+ - \gamma_{j,1}^-) p_\sigma - \gamma_{j,0}^- p_0 + \gamma_{j,1}^+ p_2,$$

where the transition rates for the heat current in Eq. (11) are given by:

$$\gamma_{j,s}^\pm = \Gamma_j \int dE (E - eV_j) f^\pm(E - eV_j) P_j(E - \mu_s). \quad (12)$$

These rates take into account the heat transported in each particle transition.

B. Linear regime

By linearizing the electrical I_i^e and heat I_i^h currents at the i -th reservoir in response to the applied thermodynamical forces $\{V_j, T_j\}$

$$I_i^e = \sum_j (G_{ij} V_j + L_{ij} T_j), \quad (13)$$

$$I_i^h = \sum_j (M_{ij} V_j + K_{ij} T_j), \quad (14)$$

we obtain the four conductance matrices that compose the Onsager matrix. Onsager-Casimir reciprocity relations dictate $G_{ij} = G_{ji}$, $K_{ij} = K_{ji}$, and $L_{ij} = M_{ji}/T$. Additional relations imposed to the cross-conductances ($L_{ij} = L_{ji}$) arise in the case where transport occurs elastically.

In our setup, the tunneling rates in Eq. (10) describe inelastic processes. Hence, they introduce energy exchange with the environment. The energy of the two terminal system is hence not conserved. In the following we analyze the effect of inelasticity on the thermal coefficients, namely L_{ij} (or M_{ji}) and K_{ij} .

C. Thermal coefficients

Thermal rectification in an isoelectric ($V_L = V_R$) two terminal conductor occurs when the heat current becomes asymmetric on the reversal of the temperature gradient. It has been discussed that is not possible in the linear regime for the heat current across the system.⁵³ One has to take into account that energy is dissipated into the environment at the nanostructure. However in an experiment this quantity is not easy to detect. One would rather measure the heat current at each terminal.

In this case, an apparent thermal rectification would be measured if

$$\delta I_{LR}^h = I_L^h(V=0, \Delta T) - I_R^h(V=0, -\Delta T) \neq 0. \quad (15)$$

If we assume that the gradient is distributed between the two terminals, i.e. $\Delta T = \Delta T_L - \Delta T_R$, we get after linearizing the currents:

$$\delta I_{LR}^h = (K_{LL} - K_{RR}) \Delta T_L + (K_{LR} - K_{RL}) \Delta T_R. \quad (16)$$

The second term of the right-hand side of Eq. (16) vanishes due to the fulfilment of the Onsager relations. This however does not apply to the diagonal coefficients, K_{LL} and K_{RR} . We will discuss below in which conditions these two coefficients become unequal in the presence of an environment, thus leading to asymmetric heat conduction.

D. Thermoelectric coefficients

It has been discussed that asymmetries of the L_{ij} coefficients might improve the thermoelectric efficiency⁷⁸. This is the case for instance for broken time reversal symmetry in the presence of a magnetic field. Then, the efficiency at maximum power depends on the ratio $L_{ij}(B)/L_{ji}(-B)$. In our device L becomes asymmetric under “contact” inversion even in the absence of magnetic field.

In this case, our system acts as an engine which generates a finite power when the thermally activated current flows against a voltage gradient. Important coefficients of performance are the maximum generated power and the efficiency at maximum power. Let us specify a configuration where $T_L > T_R$, and an applied voltage $V_R - V_L = \Delta V$. The extracted power

$$P = -I_L(\Delta V) \Delta V = I_R(\Delta V) \Delta V \quad (17)$$

is maximized for some drop voltage $\Delta V = V_m$, giving:

$$V_m = -(L_{LR} \Delta T_R + L_{LL} \Delta T_L) / (2G_{LR}), \quad (18)$$

which results in a maximum power:

$$P_{\max} = \frac{(L_{LR} \Delta T_R + L_{LL} \Delta T_L)^2}{4G_{LR}}. \quad (19)$$

Finally the efficiency at maximum power η_{\max} is easily computable from

$$\eta_{\max} = \frac{-P_{\max}}{I_L^h(V_m) + I_E^h(V_m)}, \quad (20)$$

where one has to take into account the heat current injected by the environment, I_E^h .

In order to carry a more meaningful study of the setup efficiency, we also study the Carnot efficiency for this setup. In our case we need to take into account that heat is being injected by the environment and thus the Carnot efficiency is not simply $\eta_C = 1 - T_R/T_L$. We define the Carnot efficiency at the reversible point where $\frac{I_L^h}{T_L} + \frac{I_R^h}{T_R} + \frac{I_E^h}{T_0} = 0$ (zero entropy production), which results in:

$$\eta_C = 1 + \left(\frac{I_L^h}{I_R^h} \frac{1 - T_0}{T_R} - \frac{T_0}{T_L} \right)^{-1}. \quad (21)$$

This efficiency gives a measure of the performance of our setup.

III. SINGLE OCCUPANCY

We can make some analytical progress by considering a simplified situation. Let us assume the limit $E_C \gg k_B T_0$, such that the quantum dot can be occupied by a single electron at a time. It will later help to understand the numerical results for the general configuration presented in Sec. IV. In this case, the charge current simply reads:

$$I_L^e = e \frac{\Gamma_{L,0}^+ \Gamma_{R,0}^- - \Gamma_{L,0}^- \Gamma_{R,0}^+}{\Gamma_{L,0}^+ + \Gamma_{R,0}^- + \Gamma_{L,0}^- + \Gamma_{R,0}^+}, \quad (22)$$

with $I_R^e = -I_L^e = I$. We consider the isoelectric case (we define $\Delta\mu^0 = \epsilon_d + e^2/2C$) and compute the linearized charge current in contact l by linearizing tunneling rates as follows

$$\Gamma_{l,0}^+ = \Gamma_l \left(g_l^{(0)} + \frac{\Delta T_l}{T} g_l' \right) \quad (23)$$

$$\Gamma_{l,0}^- = e^{\Delta\mu^0/kT} \left(\Gamma_l^+ - \frac{\Delta T_l}{T} \Gamma_l g_l^{(1)} \right), \quad (24)$$

where we have introduced the following integrals:

$$\begin{aligned} g_l^{(n)} &= \int dE \left(\frac{E + \Delta\mu^0}{kT} \right)^n f^+(E + \Delta\mu^0) P_l(E), \\ g_l'^n &= \frac{1}{kT} \int dE \left(\frac{E + \Delta\mu^0}{kT} \right)^n f^+(E + \Delta\mu^0) \\ &\quad \times f^-(E + \Delta\mu^0) P_l(E), \end{aligned}$$

which only depend on the corresponding terminal through the $P_l(E)$ function, $l = L, R$. In the following, we write $f^\pm(E)$ for $f^\pm(E, T)$.

Replacing them into Eq. (22) we obtain the Seebeck coefficients:

$$\begin{aligned} L_{LR} &= - \frac{e \Gamma_L \Gamma_R}{\sum_l \Gamma_l g_l^{(0)}} e^{\Delta\mu^0/kT} f^+(\Delta\mu^0) g_L^{(0)} g_R^{(1)} \\ L_{RL} &= - \frac{e \Gamma_L \Gamma_R}{\sum_l \Gamma_l g_l^{(0)}} e^{\Delta\mu^0/kT} f^+(\Delta\mu^0) g_R^{(0)} g_L^{(1)}. \end{aligned}$$

The asymmetry in the thermoelectric coefficients is hence:

$$L_{LR} - L_{RL} \propto g_L^{(0)} g_R^{(1)} - g_R^{(0)} g_L^{(1)} = X_{RL}^{(1)}, \quad (25)$$

with

$$\begin{aligned} X_{ll'}^{(n)} &= \int dE dE' \left(\frac{E + \Delta\mu^0}{kT} \right)^n f^+(E + \Delta\mu^0) f^+(E' + \Delta\mu^0) \\ &\quad \times [P_l(E) P_{l'}(E') - P_l(E') P_{l'}(E)]. \end{aligned} \quad (26)$$

We can then explicitly relate the asymmetry of the Seebeck coefficients (25) to the inhomogeneous influence of the environment on the tunneling processes through each barrier, $P_l(E)$. This occurs when $C_L \neq C_R$: both the mean and variance of the distributions become different, cf. Eq. (9). Hereafter, we parametrize the asymmetry of the tunnel barrier capacitances with

$$\kappa = \frac{C_L - C_R}{C}. \quad (27)$$

Then, for a finite κ it follows that $P_L(E) \neq P_R(E)$. Note that $X_{ll'}^{(n)}$ is independent of the tunneling rates Γ_L , and Γ_R .

The functions $X_{ll'}^{(n)}$ (and therefore the asymmetry) depend on the overlapping of the distributions $P_L(E)$ and $P_R(E)$, which depends on C . For very small capacitances, $C \rightarrow 0$, the two distributions are narrow and they do not overlap. In the opposite limit, they are so wide that their difference is tiny. In between we can therefore find optimal values of C for which the effect of the environment is maximal.

These observations are reflected in Fig. 2. There we have represented $L_{LR} - L_{RL}$ for two different values of the total capacitance $C = C_0$ [Fig. 2(a)] and $2C_0$ [Fig. 2(b)], with $C_0 = e^2/10h\Gamma_0$, as a function of the energy level of the dot ϵ_d and κ . We vary the symmetry of the capacitances described by κ but not the total capacitance C which is kept constant. As seen in Fig. 2 the difference $L_{LR} - L_{RL}$ is zero for $\kappa = 0$. This means that an environment coupled symmetrically to both barriers is not able to break this symmetry and therefore, inelastic scattering is not a sufficient condition in order to break this symmetry in the Onsager matrix. However, we observe that for a finite κ both contributions, L_{LR} , L_{RL} differ, see Fig. 2(c) and (d). Both have the expected saw-tooth lineshape⁴⁶. Remarkably, $L_{LR} - L_{RL}$ reverses its sign when $\epsilon_d - E_C$ and κ are tuned are shown in the upper pannel of Fig. 2. It changes sign when the asymmetry is

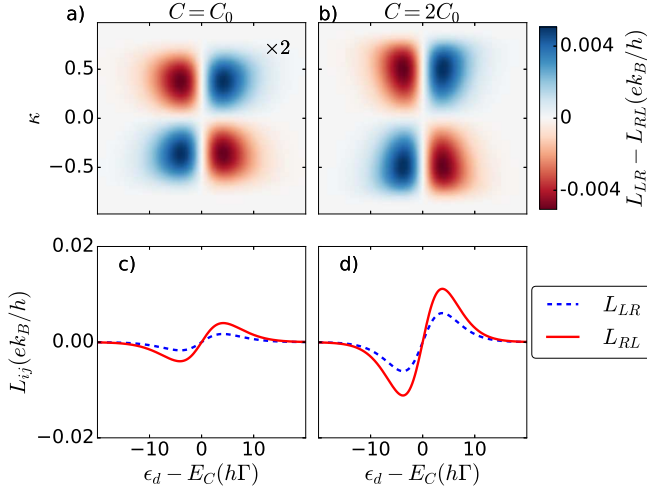


FIG. 2. Electrothermal asymmetry $L_{LR} - L_{RL}$ versus dot energy level position $\epsilon_d - E_C$ and capacitance asymmetry κ for different values of the total capacitance (a) $C = C_0$, and (b) $C = 2C_0$. (c) and (d) show cuts of L_{LR} , and L_{RL} when $\kappa = 0.5$, for the values of C considered above. We have taken $k_B T_0 = 2\hbar\Gamma_0$ and $\Gamma_L = \Gamma_R = \Gamma_0/2$. The crossed terms L_{LR} , and L_{RL} differ between themselves for $\kappa \neq 0$, i.e. ($C_L \neq C_R$).

inverted (i.e. when κ changes sign) and at the particle-hole symmetry point $\epsilon_d - E_C = 0$, where also $L_{ij} = 0$.

The maximal value of $L_{LR} - L_{RL}$ (at a finite value of κ) depend strongly on the total capacitance C . The difference $L_{LR} - L_{RL}$ increases with C . A plausible argument for such behavior is obtained by looking at the integrand of Eq. (26) that depends on the factor $P_R(E)P_L(E') - P_R(E')P_L(E)$ and accounts for the overlap between two Gaussian functions each centered at energy positions that depend on $\kappa_L^2 E_C$ and $\kappa_R^2 E_C$ (even though their widths depends on the same factor, as well), by making C high yields an overlapping between the two Gaussian functions and enhances the value for $X_{RL}^{(1)}$. For such reason, $L_{LR} - L_{RL}$ reaches lower values whenever C is smaller.

A similar analysis is performed for the thermal coefficients. Expanding the heat rates we obtain:

$$H_l^+ = \Gamma_l \left(kT g_l^{(1)} + g_l'' k\Delta T_l \right)$$

$$H_l^- = e^{\Delta\mu^0/kT} \left(H_l^+ - \Gamma_l g_l^{(2)} k\Delta T_l \right).$$

With these relations, we get the expression for the (diagonal) linear thermal asymmetry, $\delta K = K_{LL} - K_{RR}$. It can be separated in two contributions, $\delta K = \delta K_\Gamma + \delta K_\kappa$, with:

$$\delta K_\Gamma = e^{\Delta\mu^0/kT} \frac{f(\Delta\mu^0)}{\sum_l \Gamma_l g_l^{(0)}} (\Gamma_L^2 \Theta_L - \Gamma_R^2 \Theta_R) \quad (28)$$

$$\delta K_\kappa = e^{\Delta\mu^0/kT} \frac{f(\Delta\mu^0)}{\sum_l \Gamma_l g_l^{(0)}} \Gamma_L \Gamma_R X_{LR}^{(2)}. \quad (29)$$

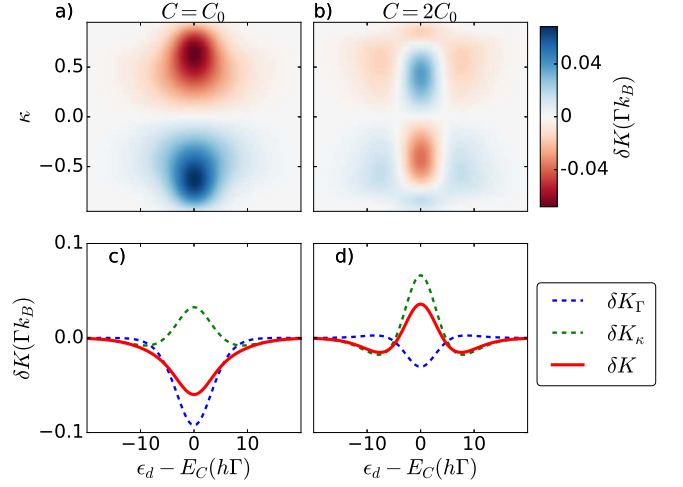


FIG. 3. a) b) Thermal asymmetry $K_{LL} - K_{RR}$ versus dot energy level position ϵ_d and capacitance asymmetry κ for different values of the total capacitance $C = C_0, 2C_0$. Heat rectification $K_{LL} - K_{RR} \neq 0$ for $\kappa \neq 0$, i.e. ($C_L \neq C_R$). c) d) Total δK (red line), tunnel δK_Γ (dashed blue line) and capacitance δK_κ (dashed green line) thermal asymmetries evaluated at $\kappa = 0.5$ for two different capacitances $C = C_0 = 2C_0$. The change of sign of δK_Γ which implies the change of sign of the total δK is clearly observed. Parameters are the same as in Fig. 2.

Here we have defined:

$$\Theta_l = -k_B T \left[\left(g_l^{(1)} \right)^2 - g_l^{(2)} g_l^{(0)} \right], \quad (30)$$

which depends on the tunneling events through a single barrier. We can hence distinguish two sources of rectification: δK_Γ becomes non zero when asymmetric tunneling barriers are considered, i.e. $\Gamma_L \neq \Gamma_R$ or when $\kappa \neq 0$. It relates to the different time scales that an electron stays in contact with the environment when tunneling from the left or from the right reservoir, as we discuss below. However, δK_κ is intrinsically dependent on the dynamic coupling to the environment: it is only non zero when the capacitances for each tunneling barrier are different.

The role of a capacitance asymmetry on the heat rectification δK is plotted in Fig. 3. There, we show $K_{LL} - K_{RR}$ versus the dot gate potential $\epsilon_d - E_C$ when the asymmetry in the capacitances κ is tuned. We observe that heat rectification reverses its sign when κ does too. Importantly, we find different behaviours depending on the total capacitance C . For large enough C , δK changes sign with the position of the level, cf. Fig. 3(b). This is due to a change in the relative contribution of the two terms, δK_Γ and δK_κ , as shown in the lower panels in Fig. 3. This effect introduces an additional way of controlling the heat flows through the device, depending on the position of the different mean values of the $P_j(E)$ distributions with respect to the Fermi energy.

For small values of C , the $P(E)$ functions of the two

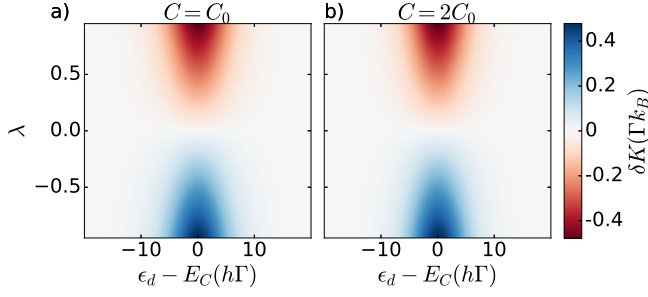


FIG. 4. Thermal asymmetry $K_{LL} - K_{RR}$ versus dot energy level position ϵ_d and barrier asymmetry λ for different values of the total capacitance $C = C_0, 2C_0$. Heat rectification $K_{LL} - K_{RR} \neq 0$ for $\gamma \neq 0$, i.e. ($\Gamma_L \neq \Gamma_R$). Parameters are the same as in Fig. 2.

contacts differ greatly and therefore δK_Γ is big (and negative for $\kappa > 0$), see Fig. 3(c). Therefore it dominates over δK_κ for $C = C_0$. Instead, for high values of C we showed that $X_{LR}^{(n)}$ enhances strongly (the two environmental $P(E)$ -functions overlap when C is high, leading to a greater contribution) and on top of that, δK_Γ has now decreased, see Fig. 3(d). Therefore, from the competition between the two terms and its dependence with κ one obtains a nontrivial dependence of the heat rectification with C .

Now we explore the heat rectification arising from different tunneling amplitudes, see Fig. 4. There, we show $K_{LL} - K_{RR}$ versus the dot gate potential $\epsilon_d - E_C$ when the asymmetry in the tunneling rate, parametrized as

$$\lambda = \frac{\Gamma_L - \Gamma_R}{\Gamma} \quad (31)$$

is tuned, with $\Gamma = \Gamma_L + \Gamma_R$. Heat rectification stems from purely different kinetic couplings. In this case δK_Γ is the only source of rectification in the heat flow. In that case, the same $P(E)$ function represent the same environment for the two barriers. However, by allowing $\Gamma_L \neq \Gamma_R$ electrons traversing the left barrier spend shorter times in contact with the environment (and therefore the time where energy-exchange processes are taken is shorter) than electrons at the other barrier. Therefore environmental assisted tunneling transitions are effectively different for both junctions even though they are performed with the same environment, with $P_L(E) = P_R(E)$. Results for $K_{LL} - K_{RR}$ at $C_L = C_R = C/2$ for different values of the barrier asymmetry λ are shown in Fig. 4. In this figure we observe that indeed for $\lambda \neq 0$ there is an asymmetry of the thermal coefficients which changes sign with λ . It is also observed that the shape of the asymmetry does not depend strongly on the total capacitance C , as expected, since the source for such heat rectification depends essentially on λ and it does not have an electrostatic origin. Even so, the total value of the rectification decreases with the capacitance.

Finally, we focus on how the thermoelectric perfor-

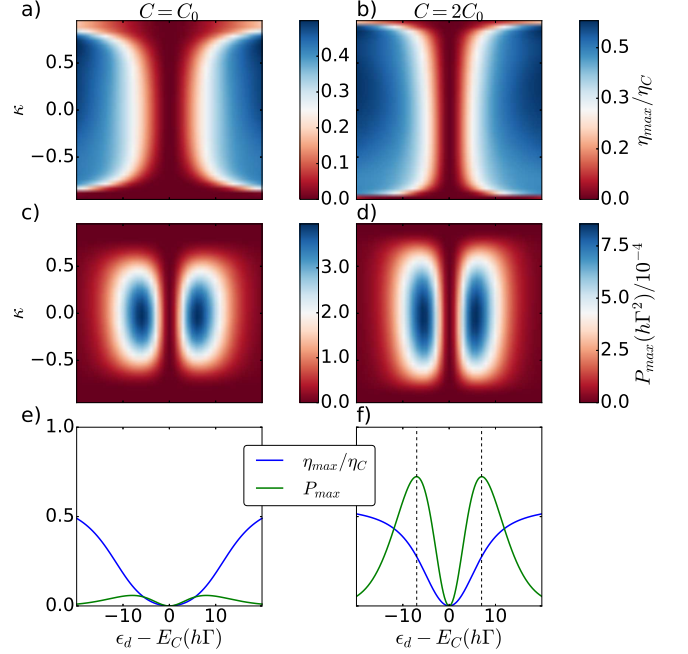


FIG. 5. Efficiency at maximum power η_{\max} in units of the Carnot efficiency η_C computed at maximum power versus the dot level position ϵ_d and the asymmetry parameter κ , for different capacitances: (a) $C = C_0$ and (b) $C = 2C_0$. (c), (d): Maximum power P_{\max} extracted corresponding at the efficiency η showed in (a) and (b), respectively. Cuts of the previous curves for $\kappa = 1/2$ are presented in (e) and (f), for clarity. Parameters are the same as in Fig. 2.

mance of the device is affected by the environment. Discrete levels in quantum dot systems are known to give a high performance for being ideal energy filters. In terms of efficiency at maximum power, they reach the Curzon-Ahlborn efficiency⁴⁴ which in the linear regime is $\eta_{CA} = \eta_C/2$ ⁷⁹. As discussed above, energy filtering is harmed by the occurrence of inelastic scattering. Hence, the efficiency is expected to be smaller⁸⁰.

This is indeed what we observe in Fig. 5, which shows the efficiency at maximum power η_{\max} [Eq. (20)] and the maximum power [Eq. (19)] as functions of the dot gate position ϵ_d and the asymmetry parameter κ . We find there that the system reaches efficiencies close to the η_{CA} bound, or even larger, cf. Fig. 5(f). This happens for large values of the dot level position and at $\kappa > 0$. The efficiency is increased whenever $C_L > C_R$ since this coupling favors the injection of heat from the environment to the right lead effectively helping electrons overcome the bias potential, therefore less heat is needed from the left reservoir to extract the same power and hence the increase in efficiency. Unfortunately, at these configurations the output power is strongly suppressed, as displayed in Fig. 5. Nevertheless, the highest P_{\max} can be extracted at reasonably high efficiencies $\eta_{\max} \sim \eta_C/3$, see Fig. 5(f). Therefore, we observed environmental en-

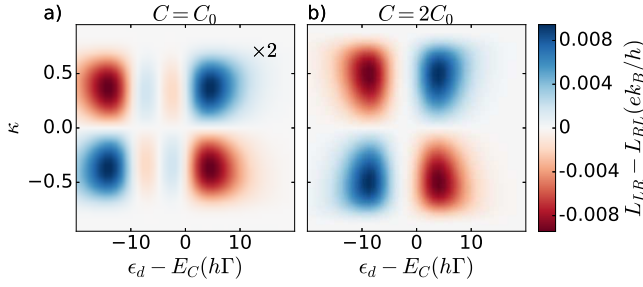


FIG. 6. Double occupancy electrothermal asymmetry $L_{LR} - L_{RL}$ versus dot energy level position $\epsilon_d - E_C$ and capacitance asymmetry κ for different values of the total capacitance $C = C_0, 2C_0$. The crossed terms L_{LR} , and L_{RL} differ between themselves for $\kappa \neq 0$, i.e. ($C_L \neq C_R$). Parameters are the same as in Fig. 2.

hanced efficiencies (as compared with a perfect energy filter⁴⁴, which are bound by the Curzon-Ahlborn limit).

We also note that the efficiency is strongly dependent on the details of the coupling to the environment, evidenced by the comparison of Figs. 5(e) and (f). Larger C not only gives larger power, it also generates it at much larger efficiencies, as compared with lower C . Hence, we expect that the engineering of the environmental fluctuations (by considering e.g. non-ohmic impedances) could result in devices with enhanced thermoelectric performances.

IV. DOUBLE OCCUPANCY

In the light of the results presented in the previous section for the reduced Hilbert space with up to one electron, we come back to the general configuration allowing for double occupancy. That is, now we consider $|0\rangle$, $|u\rangle$, $|d\rangle$ and $|2\rangle$. Analytical results for the double occupancy case are cumbersome so we restrict ourselves to present our numerical simulations. The results presented in this section show the two differences: $L_{LR} - L_{RL}$ and δK .

Firstly, we present the results for $L_{LR} - L_{RL}$ in Fig. 6. As expected, such difference arises only with an electrostatic asymmetry coupling, i.e., when $\kappa \neq 0$. Now, a second peak for $L_{LR} - L_{RL}$ appears corresponding to the charging of the system with a second electron. The two saw-tooth oscillations are separated by the charging energy $\mu_1 - \mu_0 = 10h\Gamma$, see Fig. 6(a). Notice that when the charging energy becomes sufficiently small, i.e. for $C = 2C_0$, the two features come closer and the inner oscillations are no longer visible. The behaviour then resembles the one obtained in the opposite limit (large charging energy) in Section III.

The heat rectification for the double occupancy case is plotted in Fig. 7. We observe the double peak structure for a low capacitance $C = C_0$ due to the two different energy levels available. As C increases there are two main

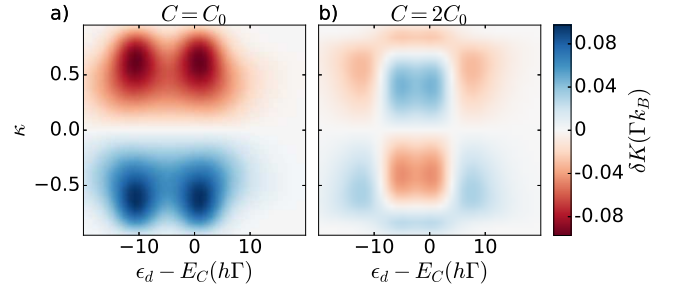


FIG. 7. Double occupancy thermal asymmetry $K_{LL} - K_{RR}$ versus dot energy level position ϵ_d and capacitance asymmetry κ for different values of the total capacitance $C = C_0, 2C_0$. Heat rectification $K_{LL} - K_{RR} \neq 0$ for $\kappa \neq 0$, i.e. ($C_L \neq C_R$). Same parameters as in Fig. 2.

effects (i) the overall double peak tends to disappear since the charging energy diminishes, and (ii) sign changes appear in the heat rectification (for fixed κ) due a greater weight of δK_κ against δK_Γ when C increases. Therefore the sign of the heat rectification is mainly given by δK_κ for a large capacitance C whereas δK_Γ determines the heat rectification sign when C is small.

V. CONCLUSIONS

In closing, we have analyzed the effect of inelasticity introduced by an electromagnetic environment on transport through a conductor (a quantum dot). We have found that even in the absence of a magnetic field, an asymmetric energy exchange with the environment can break symmetries of the transport coefficients which has a consequence the apparent occurrence of heat rectification in the linear regime. Furthermore, we have shown that heat injected from the environment can either improve or diminish the efficiency at maximum power output of the device when used as an engine. Efficiencies close to the Curzon-Ahlborn are attainable even if at vanishing power output.

We have considered here the case of a high impedance environment. Other kind of interactions will have different impact on the performance of the system. The experimental ability to engineer the electromagnetic environment⁸¹ opens the way to improve the control of thermal flows in mesoscopic conductors.

ACKNOWLEDGMENTS

We acknowledge discussions with D. Sánchez. G.R. and R.L. were supported by MINECO Grants No. FIS2014-52564. R.S. acknowledges financial support from the Spanish Ministerio de Economía y Competitividad via grant No. MAT2014-58241-P. We also thank the

- ¹ F. Giazotto, T. T. Heikkilä, A. Luukanen, A. M. Savin, and J. P. Pekola, *Rev. Mod. Phys.* **78**, 217 (2006).
- ² Y. Dubi and M. Di Ventra, *Rev. Mod. Phys.* **83**, 131 (2011).
- ³ G. Benenti, G. Casati, K. Saito, and R. S. Whitney, ArXiv e-prints (2016), [arXiv:1608.05595 \[cond-mat.mes-hall\]](#).
- ⁴ J. P. Pekola, *Nat. Phys.* **11**, 118 (2015).
- ⁵ R. Sánchez, B. Sothmann, and A. N. Jordan, *New Journal of Physics* **17**, 075006 (2015).
- ⁶ P. P. Hofer and B. Sothmann, *Phys. Rev. B* **91**, 195406 (2015).
- ⁷ P. P. Hofer, J.-R. Souquet, and A. A. Clerk, *Phys. Rev. B* **93**, 041418 (2016).
- ⁸ G. Marchegiani, P. Virtanen, F. Giazotto, and M. Campisi, *Phys. Rev. Applied* **6**, 054014 (2016).
- ⁹ J. Roßnagel, S. T. Dawkins, K. N. Tolazzi, O. Abah, E. Lutz, F. Schmidt-Kaler, and K. Singer, *Science* **352**, 325 (2016).
- ¹⁰ B. Karimi and J. P. Pekola, *Phys. Rev. B* **94**, 184503 (2016).
- ¹¹ J. Meair, J. P. Bergfield, C. A. Stafford, and P. Jacquod, *Phys. Rev. B* **90**, 035407 (2014).
- ¹² A. N. Jordan, B. Sothmann, R. Sánchez, and M. Büttiker, *Phys. Rev. B* **87**, 075312 (2013).
- ¹³ S. Donsa, S. Andergassen, and K. Held, *Phys. Rev. B* **89**, 125103 (2014).
- ¹⁴ B. Sothmann, R. Sánchez, and A. N. Jordan, *Nanotechnology* **26**, 032001 (2015).
- ¹⁵ Roche B., Roulleau P., Jullien T., Jompol Y., Farrer I., Ritchie D.A., and Glattli D.C., *Nature Communications* **6**, 6738 (2015).
- ¹⁶ F. Hartmann, P. Pfeffer, S. Höfling, M. Kamp, and L. Worschech, *Phys. Rev. Lett.* **114**, 146805 (2015).
- ¹⁷ M. Nahum, T. M. Eiles, and J. M. Martinis, *Applied Physics Letters* **65**, 3123 (1994).
- ¹⁸ M. M. Leivo, J. P. Pekola, and D. V. Averin, *Applied Physics Letters* **68**, 1996 (1996).
- ¹⁹ J. R. Prance, C. G. Smith, J. P. Griffiths, S. J. Chorley, D. Anderson, G. A. C. Jones, I. Farrer, and D. A. Ritchie, *Phys. Rev. Lett.* **102**, 146602 (2009).
- ²⁰ J. V. Koski, A. Kutvonen, I. M. Khaymovich, T. Ala-Nissila, and J. P. Pekola, *Phys. Rev. Lett.* **115**, 260602 (2015).
- ²¹ S. Kafanov, A. Kemppinen, Y. A. Pashkin, M. Meschke, J. S. Tsai, and J. P. Pekola, *Phys. Rev. Lett.* **103**, 120801 (2009).
- ²² T. Ruokola and T. Ojanen, *Phys. Rev. B* **83**, 241404 (2011).
- ²³ D. Segal, *Phys. Rev. Lett.* **100**, 105901 (2008).
- ²⁴ T. Ruokola, T. Ojanen, and A.-P. Jauho, *Phys. Rev. B* **79**, 144306 (2009).
- ²⁵ H. Thierschmann, F. Arnold, M. Mittermüller, L. Maier, C. Heyn, W. Hansen, H. Buhmann, and L. W. Molenkamp, *New Journal of Physics* **17**, 113003 (2015).
- ²⁶ M. A. Sierra and D. Sánchez, *Materials Today: Proceedings* **2**, 483 (2015), 12th European Conference on Thermoelectrics.
- ²⁷ K. Joulain, J. Drevillon, Y. Ezzahri, and J. Ordóñez-Miranda, *Phys. Rev. Lett.* **116**, 200601 (2016).
- ²⁸ R. Sánchez, H. Thierschmann, and L. W. Molenkamp, ArXiv e-prints (2017), [arXiv:1701.00382 \[cond-mat.mes-hall\]](#).
- ²⁹ O. Entin-Wohlman, Y. Imry, and A. Aharony, *Phys. Rev. B* **82**, 115314 (2010).
- ³⁰ R. Sánchez and M. Büttiker, *Phys. Rev. B* **83**, 085428 (2011).
- ³¹ J. Matthews, D. Sánchez, M. Larsson, and H. Linke, *Phys. Rev. B* **85**, 205309 (2012).
- ³² R. Sánchez, B. Sothmann, and A. N. Jordan, *Phys. Rev. Lett.* **114**, 146801 (2015).
- ³³ A. A. M. Staring, L. W. Molenkamp, B. W. Alphenaar, H. van Houten, O. J. A. Buyk, M. A. A. Mabeoone, C. W. J. Beenakker, and C. T. Foxon, *EPL (Europhysics Letters)* **22**, 57 (1993).
- ³⁴ A. Dzurak, C. Smith, M. Pepper, D. Ritchie, J. Frost, G. Jones, and D. Hasko, *Solid State Communications* **87**, 1145 (1993).
- ³⁵ A. S. Dzurak, C. G. Smith, C. H. W. Barnes, M. Pepper, L. Martín-Moreno, C. T. Liang, D. A. Ritchie, and G. A. C. Jones, *Phys. Rev. B* **55**, R10197 (1997).
- ³⁶ T. E. Humphrey, R. Newbury, R. P. Taylor, and H. Linke, *Phys. Rev. Lett.* **89**, 116801 (2002).
- ³⁷ R. Scheibner, E. G. Novik, T. Borzenko, M. König, D. Reuter, A. D. Wieck, H. Buhmann, and L. W. Molenkamp, *Phys. Rev. B* **75**, 041301 (2007).
- ³⁸ R. Scheibner, M. Knig, D. Reuter, A. D. Wieck, C. Gould, H. Buhmann, and L. W. Molenkamp, *New Journal of Physics* **10**, 083016 (2008).
- ³⁹ S. F. Svensson, A. I. Persson, E. A. Hoffmann, N. Nakpathomkun, H. A. Nilsson, H. Q. Xu, L. Samuelson, and H. Linke, *New Journal of Physics* **14**, 033041 (2012).
- ⁴⁰ S. F. Svensson, E. A. Hoffmann, N. Nakpathomkun, P. M. Wu, H. Q. Xu, H. A. Nilsson, D. Sánchez, V. Kashcheyevs, and H. Linke, *New J. Phys.* **15**, 105011 (2013).
- ⁴¹ H. Thierschmann, R. Sánchez, B. Sothmann, F. Arnold, C. Heyn, W. Hansen, H. Buhmann, and L. W. Molenkamp, *Nature Nanotechnology* **10**, 854 (2015).
- ⁴² H. Thierschmann, R. Sánchez, B. Sothmann, H. Buhmann, and L. W. Molenkamp, *Comptes Rendus Physique* **17**, 1109 (2016).
- ⁴³ G. D. Mahan and J. O. Sofo, *Proc. Natl. Acad. Sci. U. S. A.* **93**, 7436 (1996).
- ⁴⁴ M. Esposito, K. Lindenberg, and C. V. den Broeck, *EPL (Europhysics Letters)* **85**, 60010 (2009).
- ⁴⁵ D. V. Averin and K. K. Likharev, *Journal of Low Temperature Physics* **62**, 345 (1986).
- ⁴⁶ C. W. J. Beenakker and A. A. M. Staring, *Phys. Rev. B* **46**, 9667 (1992).
- ⁴⁷ M. Rey, M. Strass, S. Kohler, P. Hänggi, and F. Sols, *Phys. Rev. B* **76**, 085337 (2007).
- ⁴⁸ S. Jürgens, F. Haupt, M. Moskalets, and J. Splettstoesser, *Phys. Rev. B* **87**, 245423 (2013).
- ⁴⁹ B. Roche, R.-P. Riwar, B. Voisin, E. Dupont-Ferrier, R. Wacquez, M. Vinet, M. Sanquer, J. Splettstoesser, and X. Jehl, *Nature Communications* **4**, 1581 (2013).
- ⁵⁰ R. Sánchez, B. Sothmann, and A. N. Jordan, *Physica E*

- 75**, **86** (2016).
- ⁵¹ C. H. Schiegg, M. Dzierzawa, and U. Eckern, ArXiv e-prints (2016), [arXiv:1610.02974 \[cond-mat.mes-hall\]](#).
 - ⁵² J. Argüello-Luengo, D. Sánchez, and R. López, *Phys. Rev. B* **91**, 165431 (2015).
 - ⁵³ J. H. Jiang, M. Kulkarni, D. Segal, and Y. Imry, *Phys. Rev. B* **92**, 045309 (2015).
 - ⁵⁴ K. Yamamoto, O. Entin-Wohlman, A. Aharony, and N. Hatano, *Phys. Rev. B* **94**, 121402 (2016).
 - ⁵⁵ D. Sanchez and L. Serra, *Phys. Rev. B* **84**, 201307 (2011).
 - ⁵⁶ B. Sothmann, R. Sánchez, A. N. Jordan, and M. Büttiker, *Phys. Rev. B* **85**, 205301 (2012).
 - ⁵⁷ B. Sothmann and M. Büttiker, *EPL* **99**, 27001 (2012).
 - ⁵⁸ R. Sánchez, R. López, D. Sánchez, and M. Büttiker, *Phys. Rev. Lett.* **104**, 076801 (2010).
 - ⁵⁹ D. Bischoff, M. Eich, O. Zilberberg, C. Rössler, T. Ihn, and K. Ensslin, *Nano Letters* **15**, 6003 (2015).
 - ⁶⁰ K. Kaasbjerg and A. P. Jauho, *Phys. Rev. Lett.* **116**, 196801 (2016).
 - ⁶¹ A. J. Keller, J. S. Lim, D. Sánchez, R. López, S. Amasha, J. A. Katine, H. Shtrikman, and D. Goldhaber-Gordon, *Phys. Rev. Lett.* **117**, 066602 (2016).
 - ⁶² T. Ruokola and T. Ojanen, *Phys. Rev. B* **86**, 035454 (2012).
 - ⁶³ L. Henriet, A. N. Jordan, and K. Le Hur, *Phys. Rev. B* **92**, 125306 (2015).
 - ⁶⁴ P. Delsing, K. K. Likharev, L. S. Kuzmin, and T. Claeson, *Phys. Rev. Lett.* **63**, 1180 (1989).
 - ⁶⁵ L. J. Geerligs, V. F. Anderegg, C. A. van der Jeugd, J. Romijn, and J. E. Mooij, *EPL (Europhysics Letters)* **10**, 79 (1989).
 - ⁶⁶ M. H. Devoret, D. Esteve, H. Grabert, G.-L. Ingold, H. Pothier, and C. Urbina, *Phys. Rev. Lett.* **64**, 1824 (1990).
 - ⁶⁷ S. M. Girvin, L. I. Glazman, M. Jonson, D. R. Penn, and M. D. Stiles, *Phys. Rev. Lett.* **64**, 3183 (1990).
 - ⁶⁸ H. Grabert, G.-L. Ingold, M. H. Devoret, D. Estève, H. Pothier, and C. Urbina, *Zeitschrift für Phys. B Condens. Matter* **84**, 143 (1991).
 - ⁶⁹ H. B. G. Casimir, *Rev. Mod. Phys.* **17**, 343 (1945).
 - ⁷⁰ H. B. Callen, “Thermodynamics and an introduction to thermostatistics,” (John Wiley and Sons, New York, 1985) 2nd ed.
 - ⁷¹ P. Jacquod, R. S. Whitney, J. Meair, and M. Büttiker, *Phys. Rev. B* **86**, 155118 (2012).
 - ⁷² L. Onsager, *Phys. Rev.* **37**, 237 (1931); **37**, 405 (1931).
 - ⁷³ M. Büttiker, *IBM J. Res. Dev.* **32**, 317 (1988).
 - ⁷⁴ P. N. Butcher, *J. Phys. Condens. Matter* **2**, 4869 (1990).
 - ⁷⁵ K. Saito, G. Benenti, G. Casati, and T. Prosen, *Phys. Rev. B* **84**, 201306 (2011).
 - ⁷⁶ G.-L. Ingold and Y. V. Nazarov, “Single charge tunneling: Coulomb blockade phenomena in nanostructures,” (Springer US, Boston, MA, 1992) pp. 21–107.
 - ⁷⁷ C. W. J. Beenakker, *Phys. Rev. B* **44**, 1646 (1991).
 - ⁷⁸ G. Benenti, K. Saito, and G. Casati, *Phys. Rev. Lett.* **106**, 230602 (2011).
 - ⁷⁹ F. L. Curzon and B. Ahlborn, *Am. J. Phys.* **43**, 22 (1975).
 - ⁸⁰ N. Nakpathomkun, H. Q. Xu, and H. Linke, *Phys. Rev. B* **82**, 235428 (2010).
 - ⁸¹ C. Altimiras, O. Parlavecchio, P. Joyez, D. Vion, P. Roche, D. Esteve, and F. Portier, *Phys. Rev. Lett.* **112**, 236803 (2014).